Journal of proteome research

Article

pubs.acs.org/jpr

Metabolomics Reveals Metabolite Changes in Acute Pulmonary Embolism

Renata Bujak,[†,‡,§] Ana García-Álvarez,[⊥,∥,§] Francisco J. Rupérez,[†] Mario Nuño-Ayala,[⊥] Antonia García,[†] Jesus Ruiz-Cabello,[⊥,#] Valentín Fuster,[⊥] Borja Ibáñez,[⊥,¶] and Coral Barbas*[,†]

[†]Centre for Metabolomics and Bioanalysis (CEMBIO), Facultad de Farmacia, Universidad CEU San Pablo, Campus Monteprincipe, Boadilla del Monte 28668, Madrid, Spain

[‡]Department of Toxicology, Ludwik Rydygier Collegium Medicum in Bydgoszcz, Nicolaus Copernicus University in Torun, Torun, Poland

[⊥]Centro Nacional de Investigaciones Cardiovasculares Carlos III (CNIC)- Imaging in Experimental Cardiology Laboratory (IExC Lab), Madrid, Spain

[∥]Hospital Clínic, IDIBAPS, Barcelona, Spain

[#]Universidad Complutense de Madrid and Ciber de Enfermedades Respiratorias (CIBERES), Madrid, Spain

[¶]Hospital Clinico San Carlos, Madrid, Spain

Supporting Information

ABSTRACT: Pulmonary embolism (PE) is a common cardiovascular emergency which can lead to pulmonary hypertension (PH) and right ventricular failure as a consequence of pulmonary arterial bed occlusion. The diagnosis of PE is challenging due to nonspecific clinical presentation, which results in relatively high mortality. Moreover, the pathological factors associated with PE are poorly understood. Metabolomics can provide new highlights which can help in the understanding of the processes and even propose biomarkers for its diagnosis. In order to obtain more information about PE and PH, acute PE was induced in large white pigs and plasma was obtained before and after induction of PE. Metabolic fingerprints from plasma were obtained with LC−QTOF-MS (positive and negative ionization) and GC−Q-MS. Data pretreatment and statistical analysis (uni- and multivariate) were performed in order to compare metabolic fingerprints and to select the metabolites that showed higher loading for the classification (28 from LC and 19 from GC). The metabolites found differentially distributed among groups are mainly related to energy imbalance in hypoxic conditions, such as glycolysis-derived metabolites, ketone bodies, and TCA cycle intermediates, as well as a group of lipidic mediators that could be involved in the transduction of the signals to the cells such as sphingolipids and lysophospholipids, among others. Results presented in this report reveal that combination of LC−MS- and GC−MS-based metabolomics could be a powerful tool for diagnosis and understanding pathophysiological processes due to acute PE.

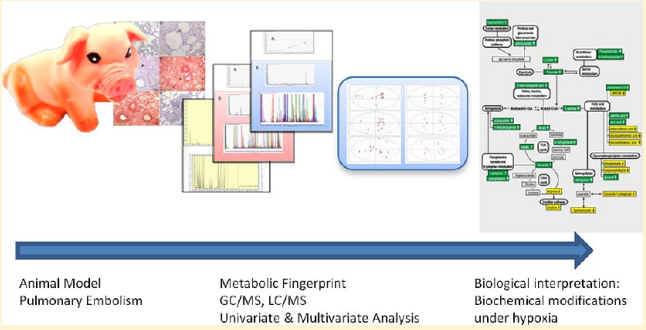

KEYWORDS: *metabolomics, metabolic fingerprinting, pulmonary embolism, pulmonary hypertension, pig*

1. INTRODUCTION

Pulmonary embolism (PE) is a relatively common cardiovascular emergency.[1] It may lead to acute life-threatening but potentially reversible pulmonary hypertension (PH) and right ventricular failure as a consequence of the occlusion of the pulmonary arterial bed. Every year around 300000 people in the United States die from acute PE, and the diagnosis is often not established until autopsy.[2] Pulmonary circulation obstruction by thrombi results in pulmonary thromboembolism (PTE) development. Additionally, lungs are a particularly common target for the embolism by other material such as air, amniotic fluid, fat, injected foreign material, or tumor.[3] This kind of embolism is called nonthrombotic pulmonary embolism (NTPE), and it is less common than PTE. The complex and multifactorial etiologies of PE result in its poor diagnosis and recognition. However, early diagnosis is crucial, since immediate treatment is very effective.

The diagnostic process of acute PE is challenging due to lack of specific clinical symptoms. Tachycardia, chest pain, cough, or unexplained syncope are usually observed in the initial stage of acute PE.[4] However, as these respiratory and chest symptoms are nonspecific and occur in many pulmonary and cardiovascular diseases, PE is very often underdiagnosed or overlooked

Received: August 26, 2013
Published: December 24, 2013

Table 1. Hemodynamic Characteristics at Baseline and 1 h after Acute PE[a]

	baseline						postacute PE					
ID	HR (bpm)	O^2 sat. (%)	mSBP (mmHg)	mPAP (mmHg)	CO (L/min)	PVR (WU)	HR (bpm)	O^2 sat. (%)	mSBP (mmHg)	mPAP (mmHg)	CO (L/min)	PVR (WU)
pig 1	77	100	100	22	5.15	2.52	91	98	94	40	3.59	8.9
pig 2	70	100	101	25	4.59	3.27	98	94	78	40	3.70	8.6
pig 3	106	100	91	19	6.55	1.52	108	87	95	45	4.70	7.7
pig 4	101	100	90	24	4.92	2.43	99	83	73	42	3.42	9.4
pig 5	66	100	67	17	2.43	1.23	96	85	64	45	2.29	17.5
pig 6	80	100	125	25	4.29	3.03	90	87	98	40	3.03	10.6
pig 7	55	100	85	15	2.76	1.09	79	91	78	41	2.42	14.4
pig 8	75	100	94	15	3.63	1.65	80	94	76	43	2.46	14.6

[a]HR, heart rate; O_2 sat., oxygen saturation, mSBP, mean systemic blood pressure; mPAP, mean pulmonary arterial pressure; CO, cardiac output; PVR, pulmonary vascular resistance.

and may result in fatal complications. Additionally, there is no single and noninvasive diagnostic test to confirm PE.[5] Among many biochemical blood parameters, determination of D-dimer level has been shown to be useful in PE diagnosis[6] because its absence may help for excluding PE. Plasma D-dimer is a specific degradation product of cross-linked fibrin, which can occur in a variety of conditions, such as cancer, necrosis, infection, or inflammation. Therefore, the specificity and positive prediction value (PPV) of D-dimer for confirmation of PE is very low.[7] Imaging techniques, like ventilation−perfusion scintigraphy, computed tomography, or pulmonary angiography, are also used as diagnostic tools of PE. Pulmonary angiography is an invasive and resource-demanding procedure; however, it presents high diagnostic accuracy.[8] Computed tomography and ventilation/perfusion scanning are examples of minimally invasive tests that can be useful for the diagnosis of PE but are also time-consuming techniques, have limited sensitivity, and require contrast agent administration and radiation. Summarizing, there is not yet a single diagnostic tool for PE which is cost-effective, accurate, and safe.

Additionally, in some patients, pulmonary artery obstruction leads to the development of chronic PH, a cause of significant mortality that is currently impossible to predict.[9] Therefore, there is a special need for searching new biomarkers in order to explain the pathomechanisms of PE and reduce its misdiagnosis.

Different animal models have been used to investigate pathomechanisms of acute PE. Current knowledge about diagnosis and treatment of PE has been obtained from experimental animal models using mostly rats or mice. However pigs, due to their genetic and metabolic similarity to humans, have been recently suggested as an important biomedical model for understanding and explaining pathological processes associated with PE.[10]The pathology can be induced by injection of polydextrane microspheres with a diameter of 300 μm, and the animals develop all the symptoms of the disease in less than one hour.[11]

Recent developments in modern technologies in system biology, such as genomics, proteomics, or metabolomics, seem to be powerful approaches in understanding pathophysiology and searching for new diagnostic biomarkers of various disorders. Metabolomics provides a comprehensive analysis of the whole metabolome under a given condition such as a pathological process, disease progression, or environmental stimuli.[12] Metabolic fingerprinting may play an important role in searching for new diagnostic biomarkers. This approach looks into a total profile, or fingerprint, as a unique pattern characterizing a metabolism in a particular case.[13] Metabolomics requires sensitive analytical techniques coupled with multivariate statistical analysis and bioinformatics tools. Nuclear magnetic resonance (NMR), gas chromatography−mass spectrometry (GC−MS), high performance liquid chromatography−mass spectrometry (HPLC−MS), and capillary electrophoresis−mass spectrometry (CE−MS) are the most common techniques applied in the metabolomics field.[14] Obviously, due to the diversity of chemical compounds present in the whole metabolome, there is not one single analytical platform allowing for estimation of all metabolites. Therefore, combination of different analytical techniques is highly recommended for high-throughput profiling.

In the herein presented study, an experimental large animal (pig) model of acute PE has been evaluated for the first time by means of an untargeted MS-based metabolic fingerprinting approach, to compare the plasma profiles obtained with liquid chromatography coupled to mass quadrupole time-of-flight MS detector (LC−MS) and gas chromatography coupled with single quad MS detector (GC−MS) before and after acute PE.

2. EXPERIMENTAL ANIMAL MODEL AND SAMPLES

Experimental procedures were performed in 2−3 month old castrated-male Large-White pigs. The study was approved by the Institutional Animal Research Committee and carried out in compliance with the Guide for the Care and Use of Laboratory Animals. Before any procedure, anesthesia was induced by intramuscular injection of ketamine (20 mg/kg), xylazine (2 mg/kg), and midazolam (0.5 mg/kg), with buprenorphine (0.3 mg/kg) for analgesia, and animals were intubated. Hemodynamic measures were obtained under mechanical ventilation (Fi O_2 35%), anesthesia maintained with intravenous midazolam (0.2 mg/kg/h) and continuous electrocardiographic and oxymetric monitoring. The right femoral artery and vein were percutaneously cannulated for continuous recording of systemic arterial pressure and pulmonary artery pressure using a Swan−Ganz catheter. Hemodynamic measurements (Table 1) included mean PA pressure, pulmonary capillary wedge pressure (PCWP) at end-expiration, and cardiac output (CO) assessed by thermodilution. Pulmonary vascular resistance (PVR) was calculated as the difference between mean PA pressure and PCWP divided by the CO in Wood units (WU).

Acute PE was generated in 8 pigs by injection of polydextrane microspheres[11] with a bead diameter of 100−300 μm (Sephadex G50 Coarse dry, Pharmacia Biotech GmbH) through the femoral vein. Animals received several doses from a suspension of 2.5 mg of microspheres per mL

dx.doi.org/10.1021/pr400872j | J. Proteome Res. 2014, 13, 805−816

with the objective to generate an increase of the mean PAP above 40 mmHg that was maintained over a period of at least 20 min, and therefore acute severe and stable PH due to PE was confirmed in all animals (Table 1).

Blood samples from all animals were obtained from the femoral vein and drawn into tubes containing lithium heparin at baseline (immediately prior to injection of microspheres), and 1 h after the beginning of the first PE procedure (in the stable phase of severe acute PH). Blood samples were centrifuged to plasma separation (30 min, 2000*g*, 4 °C), and aliquots with 500 μL of plasma were frozen at −80 °C until metabolomics analysis.

3. METABOLIC FINGERPRINTING WITH LC−MS

Sixteen pig plasma samples were analyzed by means of a metabolic fingerprinting approach using LC−MS platform. Samples were divided into two groups: plasma obtained from animals before injection of microspheres (group A), and after 1 h of PE (group B).

Plasma preparation for LC−MS analysis was performed as described previously:[15] Protein precipitation and metabolite extraction was performed by adding 1 volume of plasma to 3 volumes of a cold (−20 °C) mixture of methanol and ethanol (1:1). Samples were then vortexed for 1 min and then stored at for 5 min at 4 °C and vortexed again for a few seconds. The pellet was removed by centrifuging at 15700*g* for 20 min at 4 °C, and the supernatant was filtered through a 0.22 μm nylon filter.

Samples were analyzed by an UHPLC system (1290 Infinity series, Agilent Technologies, Waldbronn, Germany) consisting of a degasser, two binary pumps, and thermostated autosampler connected to an Agilent Technologies QTOF (6550) mass spectrometry detector. Electrospray ionization (ESI) was used as an ion source. Samples (0.5 μL) were injected onto a reversed-phase column (Zorbax Extend C18, 2.1 × 5.0 mm, 1.8 μm, Agilent Technologies) thermostated at 60 °C. The system was operated in positive and negative mode at 0.6 mL/min flow rate with solvent A, water with 0.1% formic acid, and solvent B, acetonitrile with 0.1% formic acid. Gradient started from 5% B for the first min, then to 80% in 7 min, then to 100% in 11.5 min, and returned to starting conditions in 0.5 min, keeping the re-equilibration until 15 min.

Data were collected in positive and negative ESI ion modes in separate runs. The detector operated in full scan mode from 50 to 1000 *m*/*z* for positive mode and from 50 to1100 *m*/*z* for negative mode with a scan rate of 1 scan per second. Accurate mass measurements were obtained by means of an automated calibrant delivery system using ESI source with Jet Stream technology that continuously introduced a calibration solution, with reference masses at *m*/*z* 121.0509 (protonated purine) and *m*/*z* 922.0098 [protonated hexakis(1*H*,1*H*,3*H*-tetrafluoropropoxy)phosphazine or HP-921] in positive ion mode; and *m*/*z* 112.9856 (TFA anion) and *m*/*z* 1033.9881 [hexakis(1H,1*H*,3*H*-tetrafluoropropoxy)phosphazine or HP-0921] in negative ion mode. The capillary voltage was set to 3000 V for both positive and negative ionization modes, and the nebulizer gas flow rate was 12 L/min. Randomized samples were analyzed in two separate runs (first for positive and second for negative mode).

Representative chromatograms for positive and negative mode are depicted in Figures 1S and 2S, respectively, in the Supporting Information.

4. LC−MS DATA TREATMENT AND COMPOUND IDENTIFICATION

Raw data was cleaned of background noise and unrelated ions by the Molecular Feature Extraction (MFE) tool in the MassHunter Qualitative Analysis B.05.00 software (Agilent Technologies). The MFE algorithm groups ions related by charge state, isotopic distribution, and/or the presence of adducts and dimers by using the accuracy of the mass measurements. The MFE then creates a list of all possible components as represented by the full TOF mass spectral data. Each compound is characterized by mass, retention time, and abundance. Parameters selected for data extraction by the MFE were similar to those described previously.[16,17] The background noise limit was set to 500 counts, and to find coeluting adducts of the same feature, the following adduct settings were applied: +H, +Na, +K in positive ionization, and: −H, +HCOO for negative ionization. Neutral loss of water was also included. Due to retention time shifts during LC−MS analyses, peak alignment is needed to ensure that the same entity (ideally, metabolite) is marked as the same feature within each sample. Therefore, samples were multialigned using MassProfiler Professional (B.12.01, Agilent Technologies). Parameters applied for the alignment were 0.5% for retention time correction and 20 ppm for correction of the mass. Then, before statistical analysis, a filtering step was applied to clean the data matrix from random signals and to select only features with biological meaning. Data were filtered by choosing only the features that were present in all samples in one of the compared groups (i.e., in all samples before or in all samples after pulmonary embolism).

Subsequently, accurate masses of variables representing significant differences were searched against the publicly available databases. Identification of compounds detected by LC−MS was performed by searching accurate masses of features against the data available in METLIN (www.metlin.scripps.edu), KEGG (www.genome.jp/kegg), and LIPIDMAPS (www.lipidmaps.org/), all simultaneously accessed by an in-house developed search engine, CEU MassMediator (http://ceumass.eps.uspceu.es/mediator). HMDB (www.hmdb.ca) was used, too, for complementary information. In addition, the identity of compounds obtained by databases (see above) was confirmed by LC−MS/MS by using the same QTOF. Experiments were performed with identical chromatographic conditions to the first analysis. Ions were targeted for collision-induced dissociation (CID) fragmentation on the fly based on the previously determined accurate mass and retention time. In addition, confirmation with standards was performed by comparison of retention time, isotopic distribution, and fragments of commercially (Sigma-Aldrich, St. Louis, MO, USA) available reagents with those obtain in pig plasma samples.

5. METABOLIC FINGERPRINTING WITH GC−MS

Plasma samples were prepared for GC−MS analysis as previously described.[18] Protein was precipitated with acetonitrile and separated by centrifugation (15400*g*). After the deproteinization step supernatant was transferred to another glass vial with insert and then evaporated to dryness in a Speedvac Concentrator (Thermo Fisher Scientific, Waltham, MA, USA). Derivatization was achieved in different stages: *O*-methoxyamine hydrochloride in pyridine and methoxymation was carried out overnight. BSTFA with 1% TMCS was then

dx.doi.org/10.1021/pr400872j | J. Proteome Res. 2014, 13, 805−816

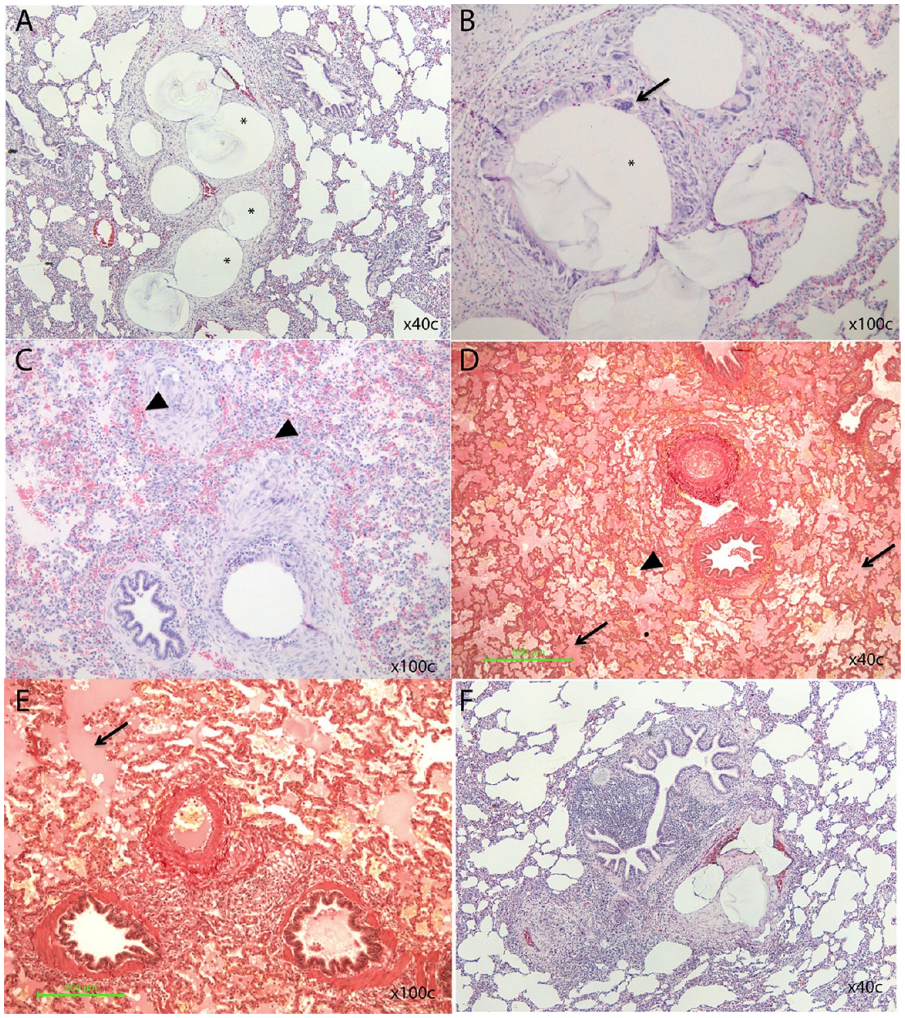

Figure 1. Example of pathology changes in lung parenchyma of distal lung lobes in a pig that underwent euthanasia 3 h after of acute pulmonary embolization. (A) Hematoxylin and eosin (H&E) staining showing vessel obstruction by several microspheres (asterisk). (B) H&E staining showing macrophages infiltration (arrow) around the microsphere obstructing the vessel. (C) H&E staining showing severe perivascular interstitial inflammatory infiltration, hemorrhage (arrowheads), and edema. (D) Picrosirius red staining showing diffuse inflammatory infiltration, hemorrhage (arrowhead), and intraalveolar edema (arrows). (E) Picrosiurius red staining showing capillary vessel occlusion, interstitial hemorrhage, and intraalveolar edema (arrow). (F) H&E staining showing severe perivascular and peribronchial inflammatory infiltration.

added, and after silylation, sample was redissolved in heptane with C18:0 methyl ester (IS).

GC−MS analyses were performed by a 7890A gas chromatography instrument (Agilent Technologies, Santa Clara, CA, USA) interfaced to inert MSD with Quadrupole (Agilent Technologies 5975). 2 μL of previously derivatized samples was injected in split mode using an Agilent Technologies 7693 autosampler onto a GC column DB5-MS (30 m length, 0.25 mm i.d., 0.25 μm film 95% dimethyl/5% diphenylpolysiloxane) with an integrated precolumn (10 m J&W) from Agilent Technologies. Carrier gas (He) flow rate was set at 1 mL/min and injector temperature at 250 °C. Split ratio was fixed from 1:5 to 1:10 with 3 to 10 mL/min He split flow into a Restek 20782 (Bellefonte, PA, USA) deactivated glass-wool split liner. Temperature gradient was programmed: Initial oven temperature was set at 60 °C (held for 1 min), then increased to 325 °C at 10 °C/min, and finally a cool-down period was applied for 10 min before the next injection. Total analysis time was 37.5 min. Detector transfer line, filament source, and quadrupole temperatures were set at 290 °C, 230 °C, and 150 °C, respectively. Voltage for electron impact (EI) ionization source was −70 eV. The mass spectrometer was operated in scan mode over a mass range of 50−600 m/z at 2 spectra/s. A representative chromatograms is depicted in Figure 3S, in the Supporting Information. Peak detection and processing of spectra were performed with ChemStation E.02.00.493 software (Agilent Technologies).

6. GC−MS DATA TREATMENT AND COMPOUND IDENTIFICATION

Data was acquired using the Agilent MSD ChemStation Software. Total ion chromatograms (TICs) were inspected according to quality of chromatograms and internal standard signal. Peak detection and deconvolution were automatically performed with Automated Mass Spectrometry Deconvolution and Identification System (AMDIS, www.amdis.net). Then, deconvoluted compounds were identified according to retention time (RT), retention index (RI), and mass spectrum. RI calculation relies on conversion of RT into constants, which are independent of system variability.

RI for each compound was obtained by normalization of its RT by the RT and RI of the closest eluting *n*-alkane, presented

dx.doi.org/10.1021/pr400872j | J. Proteome Res. 2014, 13, 805−816

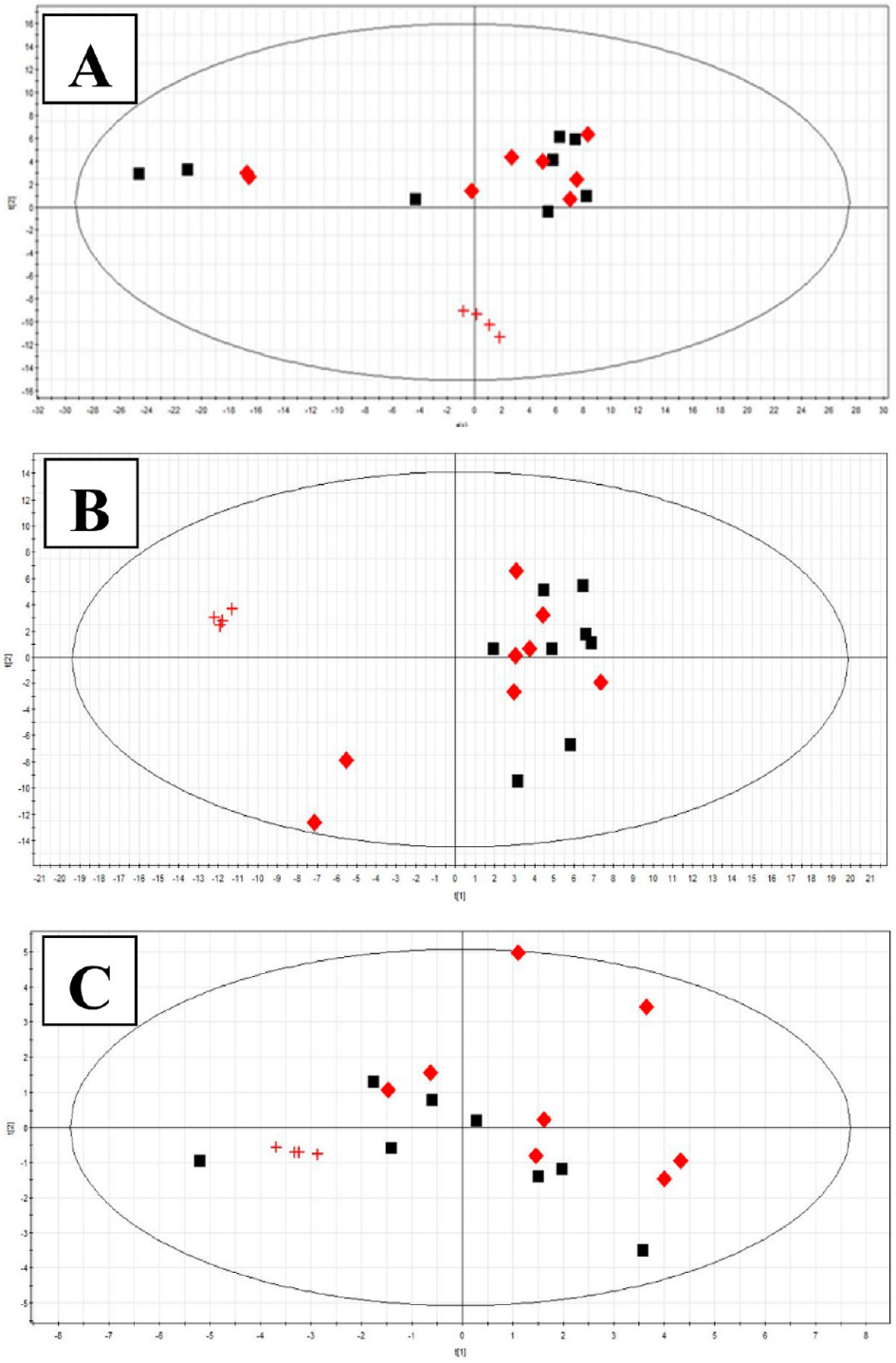

Figure 2. (A) Scores plot for a PCA model built with the data set obtained in LC−MS positive mode. Quality parameters for the model: explained variance R2 = 0.569, predicted variance Q2 = 0.451. (B) Scores plot for a PCA model built with the data set obtained in LC−MS negative mode. R2 = 0.556, Q2 = 0.308. (C) Scores plot for a PCA model built with the data set obtained in GC−MS. R2 = 0.649, Q2 = 0.368. QC samples have been marked as red crosses. Animal groups before and after acute PE have been marked as black squares or red tilted squares, respectively.

in the mix of fatty acid methyl esters, which was injected before the real samples. Based on mass spectrum and RI comparison with those from the Fiehn RTL library, the list of identified compounds was created. Additionally, mass spectra of possible compounds, which have not been found in the Fiehn RTL library, were searched through the NIST mass spectral library. According to this information, the in-house target library was created with RT and target m/z data. Multialignment was performed by MassProfiler Professional B.02.02 software (Agilent Technologies). Subsequently, filtering on frequency, sum of the derivatives, and normalization to IS were performed before statistical analysis.

7. QUALITY CONTROL AND STATISTICAL ANALYSIS

During plasma sample treatment, quality control (QC) samples were also prepared to check the stability of the LC−MS and

dx.doi.org/10.1021/pr400872j | J. Proteome Res. 2014, 13, 805−816

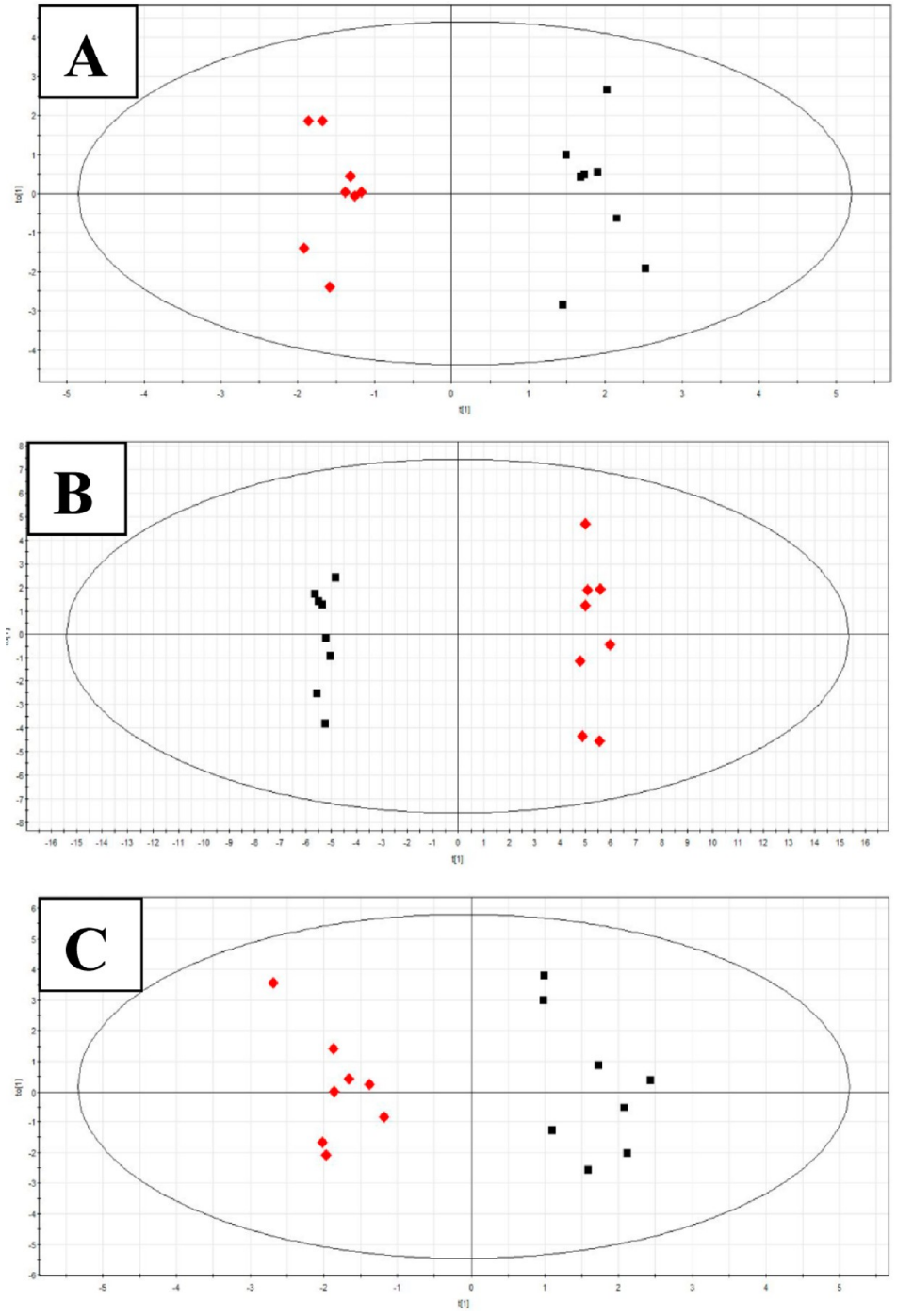

Figure 3. OPLS-DA plots plasma metabolic profiles obtained from blood before and after PE. (A) OPLS-DA model (R2 = 0.959, Q2 = 0.713) for (+) ESI-LC−MS. (B) OPLS-DA model (R2 = 0.999, Q2 = 0.984) for (−) ESI-LC−MS. (C) OPLS-DA model (R2 = 0.924, Q2 = 0.402) for GC−Q-MS. Animal groups before and after acute PE have been marked as black squares or red tilted squares, respectively.

GC−MS systems[19] during analyses of all samples, and also to control the reproducibility of the plasma sample treatment procedures. For both LC−MS and GC−MS analysis QC samples were prepared from a pool of pig plasma from other studies. Each QC sample was prepared independently following the same procedure as real samples. QCs were injected at the beginning of the run and after every 5 samples.

Comparisons between baseline (A) and one hour post PE induction (B) groups were performed with univariate and multivariate tools after filtering (see below). To find significant differences, after checking the normality of the distribution with the Lillie test, parametric or nonparametric tests were applied. In the case of parametric, standard or Welch's (according to the *F*-test for homogeneity of variances) paired *t* tests were applied. For nonparametric variables, the Mann−Whitney *U*-test was applied. The significant variables ($p < 0.05$) were log-transformed and Pareto scaled (within each set of analysis) before building independent multivariate models with SIMCA P+ 12.0.1 software (Umetrics, Umea, Sweden).

Principal components analysis (PCA), as an unsupervised multivariate analysis, was applied to check trends, outliers, and the quality of the analysis. Supervised multivariate analysis, such

dx.doi.org/10.1021/pr400872j | *J. Proteome Res.* 2014, 13, 805−816

Table 2. Compounds Significantly Changing in Pig Plasma after PE, Identified in UHPLC−QTOF-MS

name	formula	mass (DB)	RT (min)	detection mode	measured mass	mass error (ppm)	*p*-value	change B vs PE [%]	CV for QCs [%]	identification
docosatetraenoic acid	$C_{22}H_{36}O_2$	332.2715	7.4	negative	332.2719	−1.0	0.0442	−56	7	331.2641, 313.2063, 285.1474, 265.1416, 196.8666, 112.9835
docosapentaenoic acid	$C_{22}H_{34}O_2$	330.2559	7.1	negative	330.2562	−1.0	0.0341	−50	7	329.2484, 311.2605, 285.1487, 183.0122, 79.9588, 61.9881
leukotriene C4	$C_{30}H_{47}N_3O_9S$	625.3033	6.1	positive	625.2949	−3.5	0.0002	38	15	database, isotopic distribution
hydroxyoxohexadecanoic acid	$C_{16}H_{30}O_4$	286.2144	5.0	negative	286.2148	−1.4	0.0003	−25	9	285.207, 267.207, 223.2373, 160.8399
dihydroxyoctadecadienoic acid (diHODE)	$C_{18}H_{32}O_4$	312.2300	5.3	negative	312.2308	−2.4	0.0073	−106	2	367.2617, 311.1687, 183.0120, 119.0503
hydroxyoctadecenoic acid (HOME)	$C_{18}H_{34}O_3$	298.2509	5.7	negative	298.2516	−3.0	0.0235	−189	5	297.2420, 279.2270, 252.3270, 183.1352, 101.0628
oxoheptadecatrienoic acid	$C_{17}H_{26}O_3$	278.1882	5.1	negative	278.1888	−2.2	0.0081	−97	20	277.181, 259.181, 233.8374, 215.0941, 166.8653, 99.9252
dodecadienoic acid	$C_{12}H_{20}O_2$	196.1463	4.5	negative	196.1467	−2.0	0.0043	−54	6	195.1386, 176.9294, 150.8409, 136.3264, 61.9880
methyltridecanedioic acid	$C_{14}H_{26}O_4$	258.1831	4.4	negative	258.1839	−3.0	0.0002	−42	9	257.8169, 239.8047, 221.8410, 193.8308, 165.8647, 99.9248
sphingosine	$C_{18}H_{33}NO_2$	295.2511	5.0	positive	295.2526	−5.0	0.0001	79	8	296.2604, 265.0220, 207.0349, 109.1016, 95.0858
Cer(d18:1/22:0)-1P	$C_{46}H_{90}NO_{11}P$	863.6252	9.1	positive	863.6156	9.0	0.0192	−33	19	database, isotopic distribution
SM(d18:1/23:0)	$C_{46}H_{93}N_2O_6P$	800.6771	7.8	positive	800.6811	−5.0	0.0002	−60	19	801.6889, 617.6882, 225.1303, 184.0758
PC(O-40:4)	$C_{48}H_{90}NO_7P$	823.6455	10.3	positive	823.6340	14.0	0.0003	48	26	824.6418, 639.634, 184.0761, 104.1083, 86.0609
PS(36:2)	$C_{42}H_{78}NO_{10}P$	787.5363	11.4	positive	787.5386	−3.0	0.0002	−174	7	788.4817, 770.4817, 649.5179, 603.4817, 133.0878
PA(18:0/18:3)	$C_{39}H_{71}O_8P$	698.4886	9.7	negative	698.4925	−5.5	0.0315	−156	5	697.4763, 597.4763, 283.2680, 265.8536, 278.2083, 78.8820
PI(21:0/10:0)	$C_{40}H_{77}O_{13}P$	796.5102	8.7	negative	796.5075	3.3	0.0092	−154	10	795.4894, 535.6918, 325.1822, 283.2637, 241.0375, 239.8673, 212.0283, 170.9851, 116.9283
PI(21:0/13:1)	$C_{43}H_{81}O_{13}P$	836.5414	8.0	negative	836.5386	3.3	0.0002	−87	10	835.526, 575.526, 383.1867, 325.1815, 241.1342, 211.1816, 61.9879
LPE(16:0)	$C_{21}H_{44}NO_7P$	453.2855	5.5	positive	453.2864	−2.0	0.0051	−45	6	454.2932, 436.3392, 313.2734, 133.0866, 71.0860
LPE(20:4)	$C_{25}H_{44}NO_7P$	501.2855	5.3	negative	501.2888	−6.5	0.0126	−122	2	500.2750, 359.1942, 311.1664, 303.8052, 279.2308, 195.9859, 152.9990
LPI(20:1)	$C_{29}H_{55}O_{12}P$	626.3431	9.6	negative	626.3381	8.0	0.0074	−170	8	625.3371, 365.2993, 339.1993, 311.1649, 152.9269
LPA(12:0)	$C_{15}H_{31}O_7P$	354.1808	6.5	negative	354.1838	−9.0	0.0035	−56	6	353.1723, 254.1499, 199.0060, 181.0060, 155.0125, 119.0495
creatine	$C_4H_9N_3O_2$	131.0695	0.2	positive	131.0690	3.6	0.0157	−47	6	standard
arginine	$C_6H_{14}N_4O_2$	174.1117	0.2	positive	174.1126	−5.0	0.0423	−36	16	standard
alpha-tocopherol	$C_{29}H_{50}O_2$	430.3817	7.2	positive	430.3812	−0.3	0.0255	39	19	standard
didesmethyl tocotrienol	$C_{25}H_{36}O_2$	368.2715	7.3	negative	368.2728	−3.4	0.0002	−76	6	database, isotopic distribution
desmosine	$C_{24}H_{39}N_5O_8$	525.2798	5.3	negative	525.2880	−4.7	0.0021	−79	6	524.2746, 466.2871, 303.2290, 241.2146

as orthogonal partial least squares discriminant analysis (OPLS-DA), was required to select metabolites that contributed most to separation and discrimination between groups, which were selected according to the jackknife confidence intervals. Furthermore, only variables with CV <30% for LC−MS data or with CV <40% for GC−MS in the respective QC samples sets were chosen for further analysis and plottings.

8. RESULTS

Pathological changes observed in the lung parenchyma acutely after the procedure were similar to those described in patients after acute pulmonary embolization and included capillary vessel obstruction, inflammatory infiltration, and intraalveolar edema and hemorrhage (Figure 1).

Sample Classification

After alignment the respective data matrices showed 30191 and 13696 features for positive and negative LC−MS, respectively, but 94 compounds for GC−MS. LC−MS data was filtered by choosing only those features present in all samples in one of the groups, and thus the data set was reduced to 1482 for positive and 842 features for negative. After paired *t*-test, 68 variables were found significant for positive LC−MS, 78 for negative LC−MS, and they were used to build the multivariate models. For GC−MS data, all aligned variables were used for multivariate analysis.

PCA models with prediction of QC samples for LC−MS in positive mode, LC−MS in negative mode, and GC−MS are shown in Figure 2. Good cluster of the QC group and no

dx.doi.org/10.1021/pr400872j | J. Proteome Res. 2014, 13, 805−816

Table 3. Compounds Significantly Changing in Pig Plasma after PE, Identified in GC−Q-MS

name	T (target ion)	Q (qualifier ion)	RT (min)	*p*-value	change B vs PE [%]	CV for QCs [%]
pyruvic acid	174	89, 73, 59	6.584	0.025	71	19
lactic acid	117	191, 147, 73	6.749	0.042	123	10
glycerol	205	147, 117, 73	9.857	0.006	175	14
palmitic acid	313	129, 117, 73	18.813	0.037	49	36
oleic acid	339	129, 117, 75	20.403	0.021	82	35
3-hydroxybutyric acid	233	147, 117, 78	8.208	0.044	53	26
acetoacetate	89	202, 186, 59	7.806	JK	81	17
citric acid	273	347, 147, 73	16.519	JK	116	16
α-ketoglutaric acid	198	156, 147, 75	13.742	JK	85	34
fumaric acid	245	147, 75, 73	10.857	JK	114	14
malic acid	233	245, 133, 147	12.681	JK	179	28
2-hydroxybutyric acid	131	205, 147, 73	7.721	JK	105	17
pyroglutamic acid	156	230, 147, 73	13.099	JK	53	*a*
phenylalanine	120	146, 91, 75	13.466	JK	76	*a*
tryptophan	202	291, 117, 73	20.535	JK	128	*a*
2-ketoisocaproic acid	200	147, 99, 73	8.951	0.009	79	36
hypoxanthine	265	280, 206, 73	16.359	JK	96	*a*
galacturonic acid	333	292, 160, 103	17.786	0.002	229	14
β-alanine	248	248, 147, 73	11.931	JK	72	*a*

[a]CV not available. JK, Jackknife.

strong outliers according to Hottelling's T2 range plot were observed.

The results of the OPLS-DA models, displayed in Figure 3, showed clear separation of groups in both LC−MS polarity modes (Figure 3, panels A and B) and GC−MS (Figure 3, panel C). The quality of the OPLS-DA models was described by explained variance R2 (0.959 for positive, 0.999 for negative, and 0.924 for GC−MS) and predicted variance Q2 (0.713 for positive, 0.984 for negative, and 0.402 for GC−MS).

The three models were cross-validated as described previously.[15] For this analysis, one-third of the samples (n = 5) were excluded and bootstrapped thirteen times for accuracy estimation so that each training example was predicted at least once. This calculation provided the percentage of correctly classified samples and the average validation results of all prediction steps. The mean classification scores were 72 ± 14%, 96 ± 7%, and 70 ± 13% for LC−MS positive mode, LC−MS negative mode, and GC−MS, respectively. LC−MS in negative ionization mode, although using a lower number of features in the model than the positive one, showed a higher classification accuracy, and therefore could be reliably utilized to differentiate the predefined groups.

The compounds thus identified from metabolic fingerprinting are listed in Table 2 (LC−MS) and in Table 3 (GC−MS).

9. DISCUSSION

The compounds found significant can be connected by different metabolic pathways, as depicted in Figure 4. The changes herein found can be related to the pathophysiological processes involved, because PH due to PE is characterized by disturbed gas exchange which results in oxygen deficiency and leads to a hypoxia state called hypoxic pulmonary vasoconstriction.[7]

As can be seen in Tables 2 and 3 and in Figure 4, many of the significantly changed metabolites in pig plasma after acute PE are involved in the glycolysis and the tricarboxylic acid (TCA) cycle, responsible for the production of energy and the creation of primary blocks of other metabolisms. The TCA cycle converts acetyl-CoA into few intermediates and produces CO_2 and the reduced form of nicotinamide adenine dinucleotide ($NADH + H^+$) or flavin-adenine dinucleotide ($FADH + H^+$). These reduced coenzyme groups and cell oxygen are further consumed by mitochondria in oxidative phosphorylation, which is the main metabolic pathway for ATP production. In hypoxic conditions, the oxidative phosphorylation rate is reduced due to the lack of oxygen, leading therefore to the accumulation of TCA cycle intermediates. This can be described as an adaptive response to hypoxic stress, maximizing cellular energy production while protecting from adverse accumulation of ROS. In our study, the increase in citrate, malate, fumarate, and α-ketoglutarate (Table 3) could be associated with a reduced TCA cycle turnover. Solaini et al.[20] reviewed the mitochondrial metabolism under hypoxia, and Archer et al.[21] the metabolism in the right ventricle and pulmonary vasculature and suggested that impaired TCA cycle flux, by succinate dehydrogenase dysfunction and by activation of pyruvate dehydrogenase kinase, might result in decrease of energy production from both oxidative phosphorylation and TCA cycle.

The reduced rate of the TCA cycle could also lead to acetyl-CoA accumulation. In these cases of limited processing capacity of the TCA, acetyl-CoA is prompt to be consumed rather for ketogenesis. Related to this, in addition to the accumulation of TCA cycle intermediates, increased levels of β-hydroxybutyrate (β-HB) and acetoacetate (ketone bodies) after acute PE (Table 3) were found. Excess formation of β-HB is characteristic for conditions that alter the redox state of hepatic mitochondria to increase concentration of NADH. Our results showed that ketone bodies could be associated with acute PE, probably due to hypoxia-mediated alterations, and might be useful for understanding and explaining the pathogenesis of PH. Furthermore, it has been suggested that β-HB may protect the brain during hypoxia by depressing glucose uptake and consumption rather than by acting as an alternative energy substrate.[22]

A similar insight could be obtained from the differences observed with pyruvate and lactate, which were also found significantly different between groups (Table 3). The increased

dx.doi.org/10.1021/pr400872j | J. Proteome Res. 2014, 13, 805−816

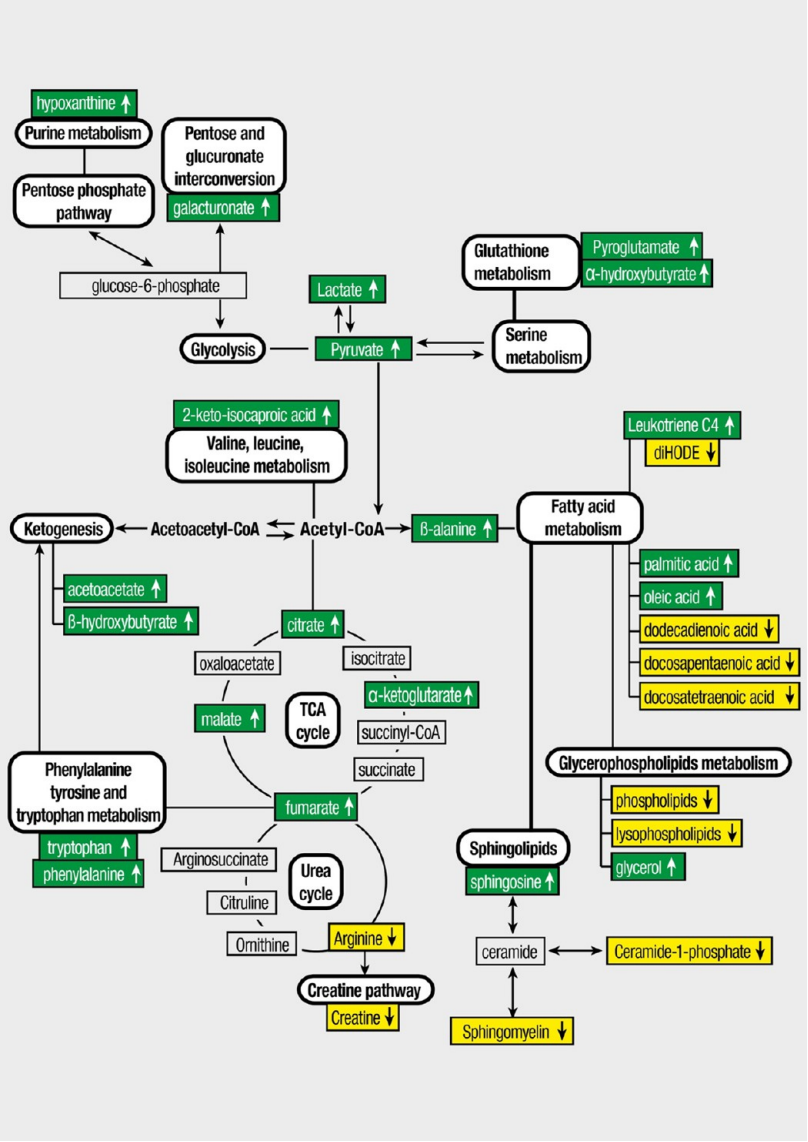

Figure 4. Metabolic changes in pig plasma after acute PE. Colored metabolites were detected using a GC−Q-MS or LC−QTOF-MS platform. Those metabolites whose concentrations were increased after acute PE are highlighted in green and those that decreased in yellow boxes.

concentration of these two metabolites in plasma of animals with acute PH due to PE could also indicate the same shift in glucose metabolism, beneficial for the generation of ATP and the prevention of mitochondrial ROS production. Oxygen level is a central regulator of balance between glycolysis and oxidative phosphorylation in the energy metabolism. Previous reports[23−25] confirmed that during hypoxia ATP generation was shifted toward glycolysis (Warburg effect) and caused cytosolic accumulation of pyruvate that could be converted to lactate by lactate dehydrogenase.[26,27]

Still, the lack of oxygen during hypoxia due to hypoxic stress in PE might lead to incomplete oxidation, excess of free radicals, and increase of glutathione consumption, which are the major intracellular antioxidants. Related to this consumption are increased levels of α-hydroxybutyrate (α-HB) and pyroglutamate (Table 3) in PE animals. α-HB is a byproduct in glutathione formation, and the relationship between the high level of this metabolite and the excess of glutathione demand, mitochondrial energy metabolism, or increased oxidative stress has been previously reported.[28] Pyroglutamate is also associated with glutathione metabolism, and its increase in hypoxic cells has been previously observed.[29]

Additionally, energy imbalance observed in our study is clearly associated with the abnormalities in lipid metabolism. The observed increase in glycerol (Table 3) and free fatty acids (FFA), such as docosatetraenoic and docosapentaenoic acids (Table 2), as well as palmitic and oleic acids (Table 3) after acute PE must be related to increase of lipolysis, as Yin et al.[30] recently suggested that hypoxia is associated with lipolysis induction in adipose tissue. Moreover, these changes could be also related to phospholipase A2 (PLA2) activity. This enzyme hydrolyzes phospholipids to free fatty acids, eicosanoids, and lysophospholipids, and as shown in Table 2, after acute PE five lysophospholipids, three phospholipids, and one phosphatidic acid were found lower, which points at regulation of the activity of PLA2, which isoforms are known to be modulated by hypoxia.[31]

FFA might provide energetic and biosynthetic substrates for signaling molecules such as oxylipins, a group of the cyclooxygenase- (COX), lipoxygenase- (LOX), and cyto-

dx.doi.org/10.1021/pr400872j | J. Proteome Res. 2014, 13, 805−816

chrome P450- (CYP) derived oxidized metabolites of polyunsaturated fatty acids (PUFA) that play a crucial role in cell proliferation, apoptosis, tissue repair, blood clotting, and inflammation. The best characterized oxylipins are prostaglandins and leukotrienes,[32] which are potent eicosanoid lipid mediators derived mainly from PLA2-released arachidonic acid. Interestingly, few oxylipins were significant discriminators between groups (Table 2). However, results did not show the same tendency for all compounds, since an increase of leukotriene C4 and a decrease in dihydroxyoctadecadienoic acid, hydroxyoctadecenoic acid, and oxoheptadecatrienoic acid was found in the group with acute PH due to PE. The initial idea that cysteinyl leukotrienes are associated with a PH mechanism was based on assessment activity of 5-lipoxygenase nonselective inhibitors or receptor agonists,[33] although this suggestion was not confirmed by later studies.[34,35]

In addition to oxylipins, differences in the levels of sphingolipids were also found between experimental groups: lower sphingomyelin and ceramide-1-phosphate (Cer-1-P) but higher sphingosine after acute PE was found in the present study (Table 2). Sphingolipids are a major class of lipid essential constituents of membranes in eukaryotes. Intensive research on their function and metabolism showed that some of them, including sphingosine, sphingosine-1-phosphate, ceramide, and Cer-1-P, are bioactive signaling molecules playing an important role in cell growth, apoptosis, signal transduction, and recognition.[36] According to previous results of Cogolludo et al.[37] that demonstrated activation of neutral sphingomyelinase (nSMase) in isolated rat pulmonary artery smooth muscle cells (PASMC) during hypoxic pulmonary vasoconstriction, the decreased level of sphingomyelin might be associated with activation of this enzyme. Cer-1-P is generated by direct phosphorylation of ceramide by ceramide kinase (CERK), and its role in cell growth and survival was recently reported.[38] It is also noteworthy that Cer-1-P is also an important mediator in inflammatory response by stimulation of cytosolic phospholipase A2 (cPLA2).[36]

Desmosine was also found lower after acute PE (Table 2). Desmosine is an amino acid involved in elastin cross-linking, and it is formed by condensation of four molecules of lysine into a pyridinum ring. Previous studies suggested that the measurement of desmosine and isodesmosine in biological fluids (urine, plasma, sputum) could be a biomarker of elastin degradation in chronic pulmonary diseases,[39,40] although its variation has not been previously reported associated with hypoxia, PE, or PH. Moreover, it has to be taken into account that these changes were found in an acute, not chronic, condition, only one hour after PE induction.

PH is a complex vascular disease, and its pathomechanism is not fully explained yet. However, there are some suggested hallmarks of PH, such as vasoconstriction, increased vascular cell proliferation, and resistance to apoptosis,[41] and these processes can be related to the stabilization of the hypoxia-inducible factor (HIF), a main transcriptional regulator of the hypoxic response known to play a predominant role in the induction of PH.[42] HIF-1α regulates many of the enzymes involved in glycolysis, which results in pyruvate dehydrogenase kinase induction, pyruvate dehydrogenase inhibition, and lactate dehydrogenase induction.[43,44] All these regulations lead to a glycolytic shift as shown in the present study (increase in pyruvate and lactate after PE, see Table 3). Furthermore, the TCA itself plays a role in the stabilization of HIF too, as the prolyl hydroxylases responsible for its degradation in normoxia are highly sensitive to the concentration of TCA cycle intermediates.[42]

Moreover, HIF-1α inhibits voltage-gated potassium (Kv) channels, which results in membrane depolarization, Ca^{2+} flux into the cells, and contractile apparatus activation.[45] In pulmonary circulation these reactions could lead to hypoxic vasoconstriction resulting in PH initiation.[41] Recent reports suggested that abnormal cellular metabolism, notably of glycolytic shift, the potential involvement of HIF-1α in this process, and alterations in mitochondrial function may be key elements in the pathogenesis of PH and could be new therapeutic targets of this disease.[24,41,46]

Moreover, HIF-1α is controlled at the transcriptional and translational level by mammalian target of rapamycin (mTOR) signaling.[47] mTOR was reported to play an important role in cell growth and regulate both anabolic and catabolic pathways in lipid metabolism,[48] and the oxylipins and lipid mediators found significantly different in the present study, known associated with pathophysiological processes as cell proliferation, cell survival, apoptosis, and cell-cycle arrest,[49] could be linked to the regulation mediated by HIF and mTOR, because the inflammation, resistance to apoptosis, and increased cell proliferation are well-known pathological features in PH development,[50] and the potential requirement of mTOR signaling pathway in cell proliferation during hypoxia-induced PH has been recently reported.[51]

Summarizing, as in tumor cells, the uncoupling between glycolysis and oxidative phosphorylation could play an important role in cell response to acute PE, could be useful to understand the pathogenesis, and may offer powerful therapeutic means to prevent or reverse disease progression at the molecular level in pulmonary hypertension.[42]

Some limitations of the study should be acknowledged. Experimental PE was generated by injection of polydextrane microspheres rather than thrombi, the most prevalent cause of human PE. The diffuse rather than segmental occlusion of pulmonary arterial bed and the composition of the microspheres might have affected metabolomics results. We acknowledge the need for further verification studies in a clinical scenario before our results can be considered validated. However, we believe that most of the acute consequences of PE that derive into metabolomics changes, such as hypoxic vasoconstriction, are common to different PE etiologies and, therefore, our results may help in the diagnosis of PE from different causes.

10. CONCLUSIONS

The observations presented here reveal that LC−QTOF-MS and GC−Q-MS-based metabolic fingerprinting could be helpful to improve diagnosis and to understand pathophysiological mechanisms related to acute PE leading to PH. Many of the metabolites significantly changed in animal group after acute PE were associated with hypoxia, lipid-related energy imbalance, and cell signaling. Therefore, abnormal cellular metabolisms such as glycolytic shift or alterations in mitochondrial function and signal transduction pathways, observed in our study, could be crucial pathological hallmarks of acute PE resulting in PH development. Further investigations using human-based biological models are needed to confirm and expand previous knowledge about pathological mechanisms and early diagnosis of PH due to acute PE. Moreover, some patients suffering from acute PE develop chronic PH and some of them do not, so prediction of chronic PH development is currently not possible.

dx.doi.org/10.1021/pr400872j | J. Proteome Res. 2014, 13, 805−816

Therefore, further studies based on large animal models of chronic PE are recommendable in order to understand pathological processes involved in PH progression in humans, and the present study shows up a group of metabolites that could be further studied and validated as diagnostic and prognostic biomarkers of the disease.

■ ASSOCIATED CONTENT

Supporting Information

Representative LC/MS (positive mode and negative mode) and GC/MS total ion chromatograms. This material is available free of charge via the Internet at http://pubs.acs.org.

■ AUTHOR INFORMATION

Corresponding Author

*E-mail: cbarbas@ceu.es. Tel: +[34] 913 724 711. Fax: +[34] 913 724 712.

Author Contributions

§Both authors shared the same amount of work.

Notes

The authors declare no competing financial interest.

■ ACKNOWLEDGMENTS

This work was supported by Spanish Ministerio de Economía y Competitividad (MINECO, previously MICINN) Grant CTQ2011-23562. The authors also acknowledge EADS-CASA for funding. Antonio de Molina was capital for the histological analysis and interpretation.

■ REFERENCES

(1) Torbicki, A.; Perrier, A.; Konstantinides, S.; Agnelli, G.; Galie, N.; Pruszczyk, P.; Bengel, F.; Brady, A. J. B.; Ferreira, D.; Janssens, U.; Klepetko, W.; Mayer, E.; Remy-Jardin, M.; Bassand, J. P. Guidelines on the diagnosis and management of acute pulmonary embolism. *Eur. Heart J.* **2008**, *29* (18), 2276−315.

(2) Tapson, V. F. Acute pulmonary embolism. *N. Engl. J. Med.* **2008**, *358* (10), 1037−52.

(3) Montagnana, M.; Cervellin, G.; Franchini, M.; Lippi, G. Pathophysiology, clinics and diagnostics of non-thrombotic pulmonary embolism. *J. Thromb. Thrombolysis* **2011**, *31* (4), 436−44.

(4) Kostadima, E.; Zakynthinos, E. Pulmonary Embolism: Pathophysiology, Diagnosis, Treatment. *Hell. J. Cardiol.* **2007**, *48* (2), 94−107.

(5) Kearon, C. Diagnosis of pulmonary embolism. *Can. Med. Assoc. J.* **2003**, *168* (2), 183−94.

(6) Di Nisio, M.; Squizzato, A.; Rutjes, A. W. S.; Buller, H. R.; Zwinderman, A. H.; Bossuyt, P. M. M. Diagnostic accuracy of D-dimer test for exclusion of venous thromboembolism: a systematic review. *J. Thromb. Haemostasis* **2007**, *5* (2), 296−304.

(7) Huisman, M. V.; Klok, F. A. Diagnostic management of clinically suspected acute pulmonary embolism. *J. Thromb. Haemostasis* **2009**, *7* (Suppl. 1), 312−17.

(8) Reinartz, P.; Wildberger, J. E.; Schaefer, W.; Nowak, B.; Mahnken, A. H.; Buell, U. Tomographic imaging in the diagnosis of pulmonary embolism: a comparison between V/Q lung scintigraphy in SPECT technique and multislice spiral CT. *J. Nucl. Med.* **2004**, *45* (9), 1501−8.

(9) Pengo, V.; Anthonie, V.; Lensing, W. A.; Prins, M. H.; Marchiori, A.; Davidson, B. L.; Tiozzo, F.; Albanese, P.; Biasiolo, A.; Pegoraro, C.; Iliceto, S.; Prandoni, P. Incidence of Chronic Thromboembolic Pulmonary Hypertension after Pulmonary Embolism. *N. Engl. J. Med.* **2004**, *350* (22), 2257−64.

(10) Barbash, I. M.; Schenke, W. H.; Halabi, M.; Ratnayaka, K.; Faranesh, A. Z.; Kocaturk, O.; Lederman, R. J. Experimental model of large pulmonary embolism employing controlled release of subacute caval thrombus in swine. *J. Vasc. Interventional Radiol.* **2011**, *22* (10), 1471−7.

(11) Böttiger, B. W.; Motsch, J.; Dörsam, J.; Mieck, U.; Gries, A.; Weimann, J.; Martin, E. Inhaled nitric oxide selectively decreases pulmonary artery pressure and pulmonary vascular resistance following acute massive pulmonary microembolism in piglets. *Chest* **1996**, *110* (4), 1041−7.

(12) Fiehn, O. Combining genomics, metabolome analysis, and biochemical modelling to understand metabolic networks. *Comp. Funct. Genomics* **2011**, *2* (3), 155−68.

(13) Shulaev, V. Metabolomics technology and bioinformatics. *Briefings Bioinf.* **2006**, *7* (2), 128−39.

(14) Lenz, E. M.; Wilson, I. D. Analytical strategies in metabonomics. *J. Proteome Res.* **2007**, *6* (2), 443−58.

(15) Ciborowski, M.; Teul, J.; Martin-Ventura, J. L.; Egido, J.; Barbas, C. Metabolomics with LC-QTOF-MS Permits the Prediction of Disease Stage in Aortic Abdominal Aneurysm Based on Plasma Metabolic Fingerprint. *PLoS One* **2012**, *7* (2), e31982.

(16) Whiley, L.; Godzien, J.; Ruperez, F. J.; Legido-Quigley, C.; Barbas, C. In-vial dual extraction for direct LC-MS analysis of plasma for comprehensive and highly reproducible metabolic fingerprinting. *Anal. Chem.* **2012**, *84* (14), 5992−9.

(17) Ciborowski, M.; Lipska, A.; Godzien, J.; Ferrarini, A.; Korsak, J.; Radziwon, P.; Tomasiak, M.; Barbas, C. Combination of LC−MS- and GC−MS-based Metabolomics to Study the Effect of Ozonated Autohemotherapy on Human Blood. *J. Proteome Res.* **2012**, *11* (12), 6231−41.

(18) Garcia, A.; Barbas, C. Gas Chromatography-Mass Spectrometry (GC-MS)-Based Metabolomics. In *Metabolic Profiling, Methods in Molecular Biology*; Metz, T. O., Ed.; Springer: New York, NY, 2011; Vol. *708*, pp 191−204.

(19) Gika, H.; Macpherson, E.; Theodoridis, G.; Wilson, I. Evaluation of the repeatability of ultra-performance liquid chromatography-TOF-MS for global metabolic profiling of human urine samples. *J. Chromatogr. B: Anal. Technol. Biomed. Life Sci.* **2008**, *871* (2), 299−305.

(20) Solaini, G.; Baracca, A.; Lenaz, G.; Sgarbi, G. Hypoxia and mitochondrial oxidative metabolism. *Biochim. Biophys. Acta* **2010**, *1797* (6), 1171−7.

(21) Archer, S. L.; Fang, Y.-H.; Ryan, J. J.; Piao, L. Metabolism and bioenergetics in the right ventricle and pulmonary vasculature in pulmonary hypertension. *Pulm. Circ.* **2013**, *3* (1), 144−52.

(22) LaManna, J. C.; Salem, N.; Puchowicz, M.; Erokwu, B.; Koppaka, S.; Flask, C.; Lee, Z. Ketones suppress brain glucose consumption. *Adv. Exp. Med. Biol.* **2009**, *645*, 301−6.

(23) Sylvester, J. T.; Shimoda, L. A.; Aaronson, P. I.; Ward, J. P. T. Hypoxic pulmonary vasoconstriction. *Physiol. Rev.* **2012**, *92*, 367−520.

(24) Leach, R. M.; Hill, H. M.; Snetkov, V. A.; Robertson, T. P.; Ward, J. P. Divergent roles of glycolysis and the mitochondrial electron transport chain in hypoxic pulmonary vasoconstriction of the rat: identity of the hypoxic sensor. *J Physiol.* **2011**, *536* (1), 211−24.

(25) Rubin, M.; Tuder, L.; Davis, A.; Graham, B. B. Targeting Energetic Metabolism. A New Frontier in the Pathogenesis and Treatment of Pulmonary Hypertension. *Am. J. Respir. Crit. Care Med.* **2012**, *185* (3), 260−6.

(26) Piao, L.; Fang, Y.-H.; Cadete, V. J. J.; Wietholt, C.; Urboniene, D.; Toth, P. T.; Marsboom, G.; Zhang, H. J.; Haber, I.; Rehman, J.; Lopaschuk, G. D.; Archer, S. L. The inhibition of pyruvate dehydrogenase kinase improves impaired cardiac function and electrical remodeling in two models of right ventricular hypertrophy: resuscitating the hibernating right ventricle. *J. Mol. Med.* **2010**, *88*, 47−60.

(27) Rehman, J.; Archer, S. L. A Proposed Mitochondrial−Metabolic Mechanism for Initiation and Maintenance of Pulmonary Arterial Hypertension in Fawn-Hooded Rats: The Warburg Model of Pulmonary Arterial Hypertension. In *Membrane Receptors, Channels and Transporters in Pulmonary Circulation, Advances in Experimental*

Medicine and Biology; Yuan, J. X.-J., Ward, J. P. T., Eds.; Springer: New York, NY, 2010; Vol. *661*, pp 171−185.
(28) Lord, R. S.; Bralley, J. A. Clinical applications of urinary organic acids. Part I: Detoxification markers. *Altern. Med. Rev.* **2008**, *13* (3), 205−15.
(29) Frezza, C.; Zheng, L.; Tennant, D. A.; Papovsky, D. B.; Hedley, B. A.; Kalna, G.; Watson, D. G.; Gottlieb, E. Metabolic Profiling of Hypoxic Cells Revealed a Catabolic Signature Required for Cell Survival. *PLoS One* **2011**, *6* (9), e24411.
(30) Yin, J.; Gao, Z.; He, Q.; Ye, J. Role of hypoxia in obesity-induced disorders of glucose and lipid metabolism in adipose tissue. *Am. J. Physiol.: Endocrinol. Metab.* **2009**, *296* (2), 333−42.
(31) Lambert, I. H.; Pedersen, S. F.; Poulsen, K. A. Activation of PLA2 isoforms by cell swelling and ischaemia/hypoxia. *Acta Physiol. (Oxford)* **2006**, *187* (1−2), 75−85.
(32) Funk, C. D. Prostaglandins and Leukotrienes: Advances in Eicosanoid Biology. *Science* **2001**, *294* (5548), 1871−75.
(33) Raj, J. U.; Chen, P. Role of eicosanoids in hypoxic vasoconstriction in isolated lamb lungs. *Am. J. Physiol.: Heart Circ. Physiol.* **1987**, *253* (3 Pt 2), 626−33.
(34) Jones, J. E.; Walker, J. L.; Song, Y.; Weiss, N.; Cardoso, W. V.; Tuder, R. M.; Loscalzo, J.; Zhang, Y. Y. Effect of 5-lipoxygenase on the development of pulmonary hypertension in rats. *Am. J. Physiol.: Heart Circ. Physiol.* **2004**, *286* (5), 1775−84.
(35) Weissmann, N.; Sommer, N.; Schermuly, R. T.; Ghofrani, H. A.; Seeger, W.; Grimminger, F. Oxygen sensors in hypoxic pulmonary vasoconstriction. *Cardiovasc. Res.* **2006**, *71* (4), 620−9.
(36) Bartke, N.; Hannun, Y. A. Bioactive sphingolipids: metabolism and function. *J. Lipid Res.* **2009**, *50* (Suppl.), 91−6.
(37) Cogolludo, A.; Moreno, L.; Frazziano, G.; Moral-Sanz, J.; Menendez, C.; Castañeda, J.; González, C.; Villamor, E.; Perez-Vizcaino, F. Activation of neutral sphingomyelinase is involved in acute hypoxic pulmonary vasoconstriction. *Cardiovasc. Res.* **2009**, *82* (2), 296−302.
(38) Geoffroy, K.; Wiernsperger, N.; Lagarde, M.; El Bawab, S. Bimodal effect of advanced glycation end products on mesangial cell proliferation is mediated by neutral ceramidase regulation and endogenous sphingolipids. *J. Biol. Chem.* **2004**, *279* (33), 34343−52.
(39) Ma, S.; Turino, G. M.; Lin, Y. Y. Quantitation of desmosine and isodesmosine in urine, plasma, and sputum by LC-MS/MS as biomarkers for elastin degradation. *J. Chromatogr. B: Anal. Technol. Biomed. Life Sci.* **2011**, *879* (21), 1893−8.
(40) Huang, J. T. H.; Chaudhuri, R.; Albarbarawi, O.; Barton, A.; Grierson, C.; Rauchhaus, P.; Weir, C. J.; Messow, M.; Stevens, N.; McSharry, C.; Feuerstein, G.; Mukhopadhyay, S.; Brady, J.; Palmer, C. N. A.; Miller, D.; Thomson, N. C. Clinical Validity of Plasma and Urinary Desmosine as Biomarkers for Chronic Obstructive Pulmonary Disease. *Thorax* **2012**, *67* (6), 502−8.
(41) Schermuly, R. T.; Ghofrani, H. A.; Wilkins, M. R.; Grimminger, F. Mechanisms of disease: pulmonary arterial hypertension. *Nat. Rev. Cardiol.* **2011**, *8* (8), 443−55.
(42) Cottrill, K. A.; Chan, S. Y. Metabolic dysfunction in pulmonary hypertension: the expanding relevance of the Warburg effect. *Eur. J. Clin. Invest.* **2013**, DOI: 10.1111/eci.12104.
(43) Agrawal, A.; Guttapalli, A.; Narayan, S.; Albert, T. J.; Shapiro, I. M.; Risbud, M. V. Normoxic stabilization of HIF-1 drives glycolytic metabolism and regulates aggrecan gene expression in nucleus pulposus cells of the rat intervertebral disk. *Am. J. Physiol.: Cell Physiol.* **2007**, *293* (2), 621−31.
(44) Marsboom, G.; Wietholt, C.; Haney, C. R.; Toth, P. T.; Ryan, J. J.; Morrow, E.; Thenappan, T.; Bache-Wiig, P.; Piao, L.; Paul, J.; Chen, C.-T.; Archer, S. L. Lung ^{18}F-Fluorodeoxyglucose Positron Emission Tomography for Diagnosis and Monitoring of Pulmonary Arterial Hypertension. *Am. J. Respir. Crit. Care Med.* **2012**, *185* (6), 670−9.
(45) Lopez-Barneo, J.; Pardal, R.; Ortega-Sáenz, P. Cellular mechanism of oxygen sensing. *Annu. Rev. Physiol.* **2001**, *63*, 259−87.
(46) Rabinovitch, M. Molecular pathogenesis of pulmonary arterial hypertension. *J. Clin. Invest.* **2012**, *122* (12), 4306−13.
(47) Land, S. C.; Tee, A. R. Hypoxia-inducible factor 1alpha is regulated by the mammalian target of rapamycin (mTOR) via an mTOR signaling motif. *J. Biol. Chem.* **2007**, *282* (28), 20534−43.
(48) Laplante, M.; Sabatini, D. M. An emerging role of mTOR in lipid biosynthesis. *Curr. Biol.* **2009**, *19* (22), 1046−52.
(49) Wymann, M. P.; Schneiter, R. Lipid signalling in disease. *Nat. Rev. Mol. Cell Biol.* **2008**, *9* (2), 162−76.
(50) Gurbanov, E.; Shiliang, X. The key role of apoptosis in the pathogenesis and treatment of pulmonary hypertension. *Eur. J. Cardiothorac. Surg.* **2006**, *30* (3), 499−507.
(51) Goncharova, E. A. mTOR and vascular remodeling in lung diseases: current challenges and therapeutic prospects. *FASEB J.* **2013**, *27* (5), 1796−807.